Rendering Lunar Eclipses

Theodore C. Yapo Barbara Cutler

Department of Computer Science
Rensselaer Polytechnic Institute

ABSTRACT

Johannes Kepler first attributed the visibility of lunar eclipses to refraction in the Earth's atmosphere in his *Astronomiae Pars Optica* in 1604. We describe a method for rendering images of lunar eclipses including color contributions due to refraction, dispersion, and scattering in the Earth's atmosphere. We present an efficient model of refraction and scattering in the atmosphere, including contributions of suspended volcanic dusts which contribute to the observed variation in eclipse brightness and color. We propose a method for simulating camera exposure to allow direct comparison between rendered images and digital photographs. Images rendered with our technique are compared to photographs of the total lunar eclipse of February 21, 2008.

Index Terms: I.3.7 [Computer Graphics]: 3D Graphics and Realism—Color, shading, shadowing, and texture; Raytracing

1 INTRODUCTION

1.1 Lunar Eclipse Phenomena

Lunar eclipses occur when the Moon passes into the Earth's shadow. Obeying a complex cycle, up to three eclipses can occur in a single year, while other years yield none at all. Unlike solar eclipses, the lunar variety can be seen from a wide area of the Earth (wherever the Moon is visible); hence, their colored and varying appearance is familiar to many amateur sky watchers.

Eclipses are categorized by the path the Moon takes through the Earth's shadow. In a *penumbral* eclipse, the Moon passes through only the outer penumbral shadow, causing a slight to moderate darkening of the lunar disk; this can be difficult to discern with the naked eye. If some part of the Moon passes into the darker umbral shadow, a partial eclipse results, while a total eclipse requires that the entire Moon pass into the umbra. Somewhat counter-intuitively, the umbral shadow is not entirely dark, but is bathed in copper-colored light which varies significantly from year to year.

The reddish color of lunar eclipses is a result of refraction and scattering in the Earth's atmosphere (Figure 1). Refraction causes sunlight to bend into the otherwise dark umbral shadow, while wavelength-dependent atmospheric scattering attenuates shorter wavelengths preferentially, leaving primarily red light to illuminate the Moon's surface (this effect is also responsible for our blue sky and red sunsets). Depending on atmospheric conditions and the Moon's path through the shadow, the appearance of the eclipse can vary significantly. The great variability of eclipse appearance is captured in the five-point Danjon observation scale [8, 10]:

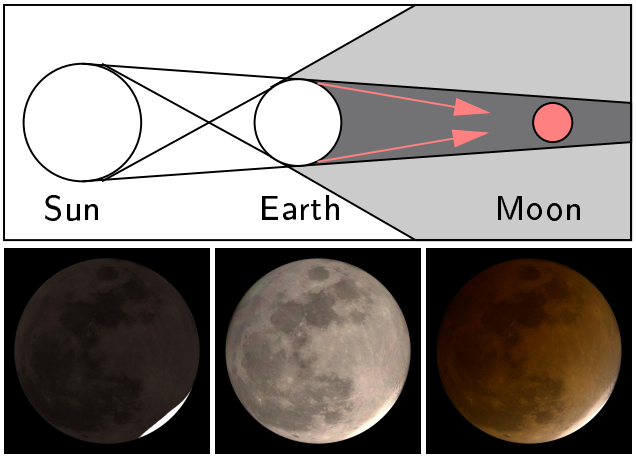

Figure 1: Lunar eclipses for different lighting models. Left: we simulate the Earth with no atmosphere; here, when the moon passes into the umbral shadow it is illuminated only by starlight, causing an extremely dark eclipse. Center: refraction by the atmosphere causes some light to be bent into the umbral shadow, which illuminates the moon. Right: atmospheric scattering attenuates shorter wavelengths, leaving primarily red light, and causing the characteristic copper eclipse color. (Upper illustration not to scale.)

L = 0	Very dark eclipse. Moon almost invisible, especially at mid-totality.
L = 1	Dark eclipse, gray or brownish in coloration. Details distinguishable only with difficulty.
L = 2	Deep red or rust-colored eclipse. Very dark central shadow, while outer edge of umbra is relatively bright.
L = 3	Brick-red eclipse. Umbral shadow usually has a bright or yellow rim.
L = 4	Very bright copper-red or orange eclipse. Umbral shadow has a bluish, very bright rim.

Even within a single eclipse, subtle variations may present themselves. Minnaert [31] gives excellent observational descriptions of many atmospheric phenomena in his classic work, and describes eclipse color variations thusly:

> "At times this is observed to consist of rings of coloured successively bright sea-green, pale golden, copper, peach-blossom pink (from the inner part outwards)."

We have developed and implemented a rendering system that can simulate these phenomena. To our knowledge, no one has previously rendered lunar eclipses.

1.2 Related Work in Astronomy & Atmospheric Science

The observed color and brightness of lunar eclipses has historically drawn scientific interest as indicators of variations in atmospheric conditions [26, 17, 37, 28, 19, 22]. Link [26] gives a detailed account of early models and presents a method for estimating illu-

minance during an eclipse using a combination of empirical and theoretical methods. Hansen and Matsushima [17] extend Link's model to include contributions of stratospheric dust and compared their results with measurements at three wavelengths taken during the December 1963 eclipse. Keen [22] explores the relationship between volcanic activity preceding historical lunar eclipses and observed eclipse brightnesses. Recent work includes measurements of absolute luminance during eclipses and comparison with calculated models [18]. Vollmer, et al. [40] describe a model for irradiance during eclipses and mapping of regions of the atmosphere which illuminate various parts of the umbra using a pinhole model.

1.3 Related Work in Computer Graphics

Several areas of previous research apply to eclipse modeling. Jensen and colleagues [21, 20] rendered various phenomena in the night sky. These effects range from accurately rendering the Moon, planets, and stars, to very subtle effects, such as the Zodiacal light. They note that their illumination model does not accurately model eclipses, however.

Other researchers have investigated issues relevant to rendering general atmospheric scenes. Gutierrez et al. [15] describe two classes of previous work for simulating atmospheric phenomena: those related to absorption and scattering, and those related to refraction. In order to simulate lunar eclipses, both must be used.

Klassen [24] describes modeling the color of the sun and sky based on a model for Rayleigh scattering. Preetham et al. [34] present an efficient model for daylight under various conditions, including effects due to atmospheric absorption and scattering.

Refraction in the atmosphere is due to varying gas density, and hence refractive index, caused by gravitational attraction between atmospheric gases and the Earth's mass. Several algorithms have been proposed for rendering scenes involving similar inhomogeneous media. Berger and Trout [3] proposed a simple model for rendering mirages, such as those described in Minnaert [31]. In their model, discrete layers of gas with different refractive indices are stacked together. Light rays are bent as they pass from one layer to another, while traveling in straight lines within each layer.

Several researchers have explored tracing rays in continuously-varying inhomogeneous media [13, 36, 14, 15, 35]. Stam and Lenguenou [36] derived equations for the trajectories of light rays in such media. The curved path of a light ray is approximated with a perturbation method based on Taylor series expansion. Gutierrez et al. [14] introduced a two-pass algorithm for inhomogeneous media called curved photon mapping and used the method to simulate the green flash phenomenon [31]. In this method, instead of back-tracing curved rays to light sources (which is difficult), diffuse photon mapping is used to simulate global lighting effects. Ray trajectories are computed by numerical integration. Gutierrez et al. [15] used a similar method, combined with a model of atmospheric inhomogeneities to model various phenomena, including mirages, the Fata Morgana, and the green flash. Seron et al. [35] rendered sunsets by solving for curved light trajectories in inhomogeneous atmospheres using a discrete-difference model.

Rayleigh scattering is due to interactions between light and small particles, including gas molecules [31]. Simulating this phenomenon has also been explored in the graphics literature. Glassner's tomes on image synthesis [12] give a good overview of the problem. Nishita et al. [32] render images of the Earth as viewed from outer space. Both Rayleigh and Mie scattering are modeled using look-up tables for efficiency. Since Rayleigh scattering is much more wavelength-dependent than Mie scattering, it is primarily responsible for the color shifts associated with scattering phenomena. Finally, Haber, et. al [16] use a method similar to ours to render twilight atmospheric effects on Earth.

2 Physical Model

2.1 The Sun

We model solar radiation at 200 different wavelengths uniformly distributed between 380 and 780 nanometers, covering roughly the entire visual spectrum. Rays are traced as "photons" that comprise a wavelength and an intensity value. For each photon, we choose a uniformly distributed random wavelength from this set, then use an initial intensity based on the ASTM E490 Solar Spectral Irradiance Tables [2] that model the extra-terrestrial solar spectrum.

2.2 Solar System Model

We model the Sun, Earth, and Moon as spheres, with radii of 6.955×10^8, 6.378×10^6, and 1.737×10^6 meters, respectively. Our eclipse simulation is driven by a date and time expressed in Coordinated Universal Time (UTC). Using the time, we calculate the configuration of the eclipsing bodies according to formulae in Meeus [29, 30]. We compute all positions relative to ecliptic coordinates, an Earth-centric spherical coordinate system defined by the plane of the Earth's rotation around the Sun. Additionally, we calculate the orientation of the moon in ecliptic coordinates to align the lunar texture map with the model. Finally, a local rotation of the moon matches the view of the eclipse as seen from Earth.

To model a particular eclipse, we calculate the position of the Sun in ecliptic coordinates for the time of greatest eclipse. We note that the size of the umbral and penumbral cones of the Earth's shadow depend only on the Sun-Earth distance, since we have not modeled the relatively small surface features of the Earth. During the few hours of the eclipse this introduces negligible error, yet allows a single set of photons to be used for rendering images at all stages of the eclipse — a significant computational savings.

2.3 Atmosphere

The atmosphere can be roughly divided into a number of layers that can be described by a piecewise model for precise calculations. We adopt the 1976 US Standard Atmosphere [38], which has previously been used to model atmospheric rendering effects [15] and correct estimated star positions for effects of atmospheric refraction [39, 41]. This model relates pressure and temperature at a given altitude to that at sea level. We use 15°C and 1013.25 mb as the mean surface temperature and pressure at sea level, respectively. Given these values, we can calculate the relative atmospheric density for any altitude, which is used it to derive the two key atmospheric quantities for our model: the molecular number density and the index of refraction, as described in Sections 2.4 and 2.5.

Many variables other than altitude affect the scattering and refractive properties of the atmosphere; most important are varying temperature, relative concentrations of the constituent gasses, including water vapor, and atmospheric aerosols such as volcanic dust. In some rendering applications, local variations in atmospheric conditions can have a dramatic effect on the result. Gutierrez et al. [15, 14] for instance, use a locally-varying atmosphere to render such phenomena as mirages, rippling sunsets, and the green flash. To render convincing lunar eclipses, such local variations are unnecessary; a uniform atmospheric profile works well. Global-scale condition changes can have dramatic effects, however. Specifically, we model global effects of stratospheric aerosols, since they represent the most significant variations in eclipse appearance [22].

We choose 42km as the maximum extent of the atmosphere; this corresponds to a density less than 0.1% of that at sea level. Rays passing through the atmosphere at higher altitudes are not refracted appreciably, and do not contribute significantly to illumination in the umbral cone. To avoid introducing a discontinuity at 42km, we taper the atmospheric density to zero over the range of 39-42km using a linear ramp. Outside this "cutoff radius," we trace rays in straight lines using a traditional ray-tracer.

2.4 Inhomogeneous Refraction

Light traveling through a media with a continuously varying refractive index is bent into a curved path. Seron et. al [35] give a numerical solution to the differential equation describing a ray's path through an inhomogeneous medium:

$$\frac{d}{dl}\left(n\frac{dx_j}{dl}\right) - \frac{\partial n}{\partial x_j} = 0,\ j \in \{0,1,2\} \tag{1}$$

where l is arc length, n the refractive index, and x the spatial coordinates of points along the light path. By discretizing Equation 1, the following relation is obtained:

$$\frac{dx_{j,i+1}}{dl} = \frac{n_i \frac{dx_{j,i}}{dl} + \frac{\partial n}{\partial x_j}\Delta l_i}{n_{i+1}}. \tag{2}$$

We use Equation 2 to find the direction of the curved ray at each step, then advance by Δl along this direction. We approximate the gradient of $n(x)$ numerically by:

$$\frac{\partial n}{\partial x_j} \approx \frac{n(x_j + \Delta x_j) - n(x_j)}{\Delta x_j} \tag{3}$$

In practice, we found that a value of 10m works well for Δx_j.

We use a fixed step size, Δl_i = 1km, to trace rays through the atmosphere. On average, 981 iterations of the curved tracing algorithm are performed per photon packet. Our experiments revealed that the total refraction (angle between a ray entering and leaving the atmosphere) was negligably affected when smaller step sizes were used, while larger step sizes caused ray trajectories to deviate.

The index of refraction of air is a function of wavelength (i.e. it is a *dispersive* media), causing various wavelengths to take different paths through the atmosphere. For a particular wavelength λ, we first calculate the index of refraction at sea level using Cauchy's equation and coefficients from the CRC Handbook [9]:

$$n_0(\lambda) \approx 1.00027643 + \frac{1.2288 \times 10^{-1}}{\lambda^2} + \frac{3.555 \times 10^4}{\lambda^4}, \tag{4}$$

with λ in nanometers. To model the effect of altitude on refractive index, we employ the Gladstone-Dale relation [15], taking the refractivity to be proportional to the density ratio:

$$n(h,\lambda) = 1 + (n_0(\lambda) - 1)\frac{\rho(h)}{\rho_0}, \tag{5}$$

where $\rho(h)$ is the calculated atmospheric density at altitude h and ρ_0 is the density of air at sea level.

2.5 Atmospheric Scattering

Light passing through the atmosphere is scattered by particles of various sizes. For particles that are small relative to the wavelength of light, the Rayleigh approximation holds. Rayleigh scattering can be modeled as an extinction process that attenuates direct-illumination rays, since the scattering direction is distributed over a broad "lobe" of angles. In contrast, scattering by larger particles is more accurately modeled by Mie scattering, which is less wavelength-dependent and has a more directional angle dependence. Hansen et al. [17] note that umbral illumination due to scattering is significant relative to direct illumination only for the darkest eclipses. Hence, we model Rayleigh scattering for direct-illumination rays exclusively, and do not consider Mie or multiple scattering phenomena. We model atmospheric scattering as a wavelength-dependent attenuation of light, according to the Beer-Lambert law. The attenuation due to Rayleigh scattering along a curved path, l, through the atmosphere can be expressed by:

$$I = I_o \exp(-\tau_l), \tag{6}$$

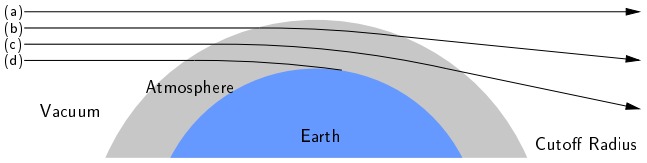

Figure 2: Tracing rays through the Earth's atmosphere. (a) Outside of the specified "cutoff radius" (> 42 km), light travels in straight lines through the vacuum of space, calculated using a traditional ray-tracer. (b&c) Once inside the atmospheric shell, light follows a curved path due to refraction through an inhomogeneous medium; a curved ray-tracer must be used. Upon leaving the shell, light again follows straight lines. (d) Some curved paths (< 5 km) terminate at the surface of the Earth contributing to colorful sunsets and sunrises. Atmosphere not drawn to scale.

where τ_l is the *optical depth* of the path. Optical depth is calculated by integration of the Rayleigh volume scattering coefficient, β:

$$\tau_l(\lambda) = \int_l \beta(\lambda,h)dl. \tag{7}$$

To calculate β, we first compute the Rayleigh scattering cross-section as given by Bucholtz [4]:

$$\sigma(\lambda) = \frac{24\pi^3(n_s^2-1)^2}{\lambda^4 N_s^2(n_s^2+2)^2}F_k \tag{8}$$

where n_s is the refractive index at the given wavelength, N_s is the molecular number density, and F_k is the King correction factor. Since F_k varies less than 0.3% over the range of visible wavelengths [4], we use a fixed value of $F_k = 1.050$ for our calculations.

The Rayleigh volume-scattering coefficient for a given wavelength and altitude is calculated by:

$$\beta(\lambda,h) = N(z)\sigma(\lambda) \tag{9}$$

where $N(h)$ is the molecular number density at altitude h, which we calculate by:

$$N(h) = N_0\frac{\rho(h)}{\rho_0}. \tag{10}$$

In practice, we assume the scattering coefficient is constant over our 1km step size, hence we attenuate the rays at each step by:

$$I_{j+i} = I_j \exp(-\beta_j \Delta l), \tag{11}$$

where β_j is the volume scattering coefficient at the beginning of the step, and I_j and I_{j+1} are the intensities at the beginning and end of the step, respectively.

2.6 Atmospheric Attenuation

The great variation in lunar eclipse brightness has been studied for centuries, with Kepler first attributing the extremely dark eclipse of 1588 to "mists and smoke" in the atmosphere. Keen [22] describes a correlation between aerosols in the stratosphere and the overall brightness of lunar eclipses, the effect of which was first attributed to volcanic eruptions after the eruption of Krakatoa in 1883. To capture this attenuation, we model a stratospheric layer of dust particles between 15 and 20km in altitude, as hypothesized by Keen. In our model, this layer uniformly attenuates all wavelengths. In the absence of data for the concentration and composition of dust particles during any particular eclipse, we propose a simple model for attenuation in this layer, taking the extinction coefficient of the layer, α, as a parameter for the model. This parameter captures losses due to both scattering and absorption in the layer; outside

Figure 3: Exploiting symmetry of the Sun-Earth system. Illumination during a lunar eclipse is symmetric relative to the center line connecting the Sun and Earth, and is independent of the Moon's position. Any ray exiting the Earth's atmosphere could have exited from any point along a circle lying in the spherical shell of the atmosphere; these rays form a hyperboloid of revolution when rotated about the symmetric axis. This illustration is drawn to scale (the Sun is 48m to the left of this page).

this layer we take $\alpha = 0$. We combine the attenuation effects of both Rayleigh scattering and extinction in the dust layer to arrive at the update rule for a photon's intensity at each time step, j:

$$I_{j+1} = I_j \exp(-(\alpha + \beta_j)\Delta l). \tag{12}$$

We found that $\alpha = 10^{-6}$ yielded only slight darkening, perhaps L4 on the Danjon scale, and $\alpha = 10^{-4}$ produced an L0 eclipse or less.

3 Rendering Method

3.1 Photon Tracing

To create the photon map for illuminating the umbral cone, we employ Monte Carlo ray tracing to cast photons starting from the Sun. A random position on the Sun's photosphere is then chosen as the origin of the photon. To cast rays efficiently, we must aim carefully; the cross-section of our 42km high atmosphere is only 1.3% of the total cross-section of the Earth as seen by the sun. Once the ray enters the atmosphere, its curved path is traced using the method of Section 2.3 until it terminates on the ground or leaves the atmosphere. All rays leaving the atmosphere are stored in a data structure for subsequent renderings of the eclipse.

Since tracing rays through the atmosphere is expensive, we use the symmetry of the Sun-Earth system to multiply the number of effective photons traced. As shown in Figure 3, the illumination produced by the Sun-Earth interaction is symmetric about the central axis of the system, hence photons can be re-used by creating multiple copies revolved around the axis of symmetry. Practically, photons can be replicated about 100 times with no appreciable artifacts; above factors of 1000, visual banding of the illumination map becomes apparent. We note that a 1D illumination map could be used for spherically symmetric atmospheres; we chose a 2D map for simplicity at the cost of a modest amount of extra memory.

3.2 Illumination Map

For each rendered image of the eclipse, we first calculate the position and orientation of the moon in ecliptic coordinates for a given time in UTC. We then calculate the intersection of all original and replicated photons with the lunar sphere, and record their contribution in an illumination map. Since each ray is of a specific wavelength, we store a spectral distribution in each pixel of the illumination map. To remove the grainy appearance that can occur due to undersampling, we convolve the map with a small Gaussian kernel.

3.3 Direct Illumination

Light reaching the Moon during a lunar eclipse can be decomposed into two components, direct and indirect. Direct illumination arrives from the Sun traveling through the vacuum of space without interaction with the Earth's atmosphere. During the partial phase of a lunar eclipse, the Moon receives some fraction of its illumination by these direct means. We model direct illumination with a second Monte Carlo method. Light rays are traced from pixels in the illumination map toward the Sun, recording the fraction of rays not occluded by the Earth, including the 42km atmospheric shell. This calculation uses a traditional ray tracer (rather than the curved ray tracer) and thus accounts for a small fraction of total computation time. The resulting model allows us to render eclipse images given a time, viewing location, and exposure length.

3.4 Rendering Spectral Distributions

At each point in the illumination map, we store an accumulator of intensities at each wavelength. To render this representation, it must first be converted to a three-color model. To do this, we implemented a method for converting a spectral distribution of light into an sRGB [1] color triplet. We first convert from wavelength and intensity to a CIE XYZ-space color triplet using tabulated CIE 1931 2° standard observer color matching functions [5]. Finally, we transform the XYZ coordinates into linear sRGB space and apply the piecewise non-linear sRGB gamma curve [1].

3.5 Rendering the Moon

The unique optical properties of the lunar surface are responsible for its peculiar appearance. Jensen et al. [20] give a model for the BRDF of the moon, which is responsible for the fact that the moon shows no "limb darkening", and hence looks more like a flat disk than a sphere in the sky. While the BRDF is convenient for lighting the moon given a light direction and angle, we instead are casting photons at the surface of the moon, which naturally simulates a Lambertian law due to foreshortening of illumination map pixels with increasing incidence angle. Rather than invert this BRDF, we simulate the flat appearance of the moon by applying a transformation that partially "undoes" the inherent Lambertian assumption. Given illumination value I_{ij} in the illumination map, we compute:

$$I'_{ij} = I_{ij}\left(\frac{1}{0.1 + 0.9\cos\theta}\right), \tag{13}$$

where θ is the angle between the incident photon and the lunar surface normal at the illumination map pixel.

The moon itself has a reddish hue, which contributes to the color of lunar eclipses, as well as that of the non-eclipsed moon. To model the average lunar albedo, we fit a second-degree polynomial to the reflectance spectrum of lunar samples obtained on the Apollo 16 mission [33]. The resulting model fits the 81 data points between 380 and 780nm to within a maximum of 0.3% error, and relates the average lunar reflectance coefficient, k_r to wavelength, λ (in nm):

$$k_r(\lambda) = -0.27063 + 2.6175 \times 10^{-03}\lambda - 1.2673 \times 10^{-06}\lambda^2.$$

The model is normalized to have a reflectance of 1.0 at 780nm. Jensen et al. [20] describe a linear model for the spectrum of the lunar albedo, which we note underestimates the green wavelengths.

We render the moon by rasterization of a pre-lit texture map on a spherical model. During a lunar eclipse, we view the moon from nearly the same angle as the illumination reaching its surface; thus, few shadows are visible, contributing to the low contrast and drab, however bright, appearance of the full moon. As a consequence, bump mapping for modeling craters and other surface features adds little visible detail when the eclipse is viewed from a position on the Earth, and these effects can be safely ignored. We note that

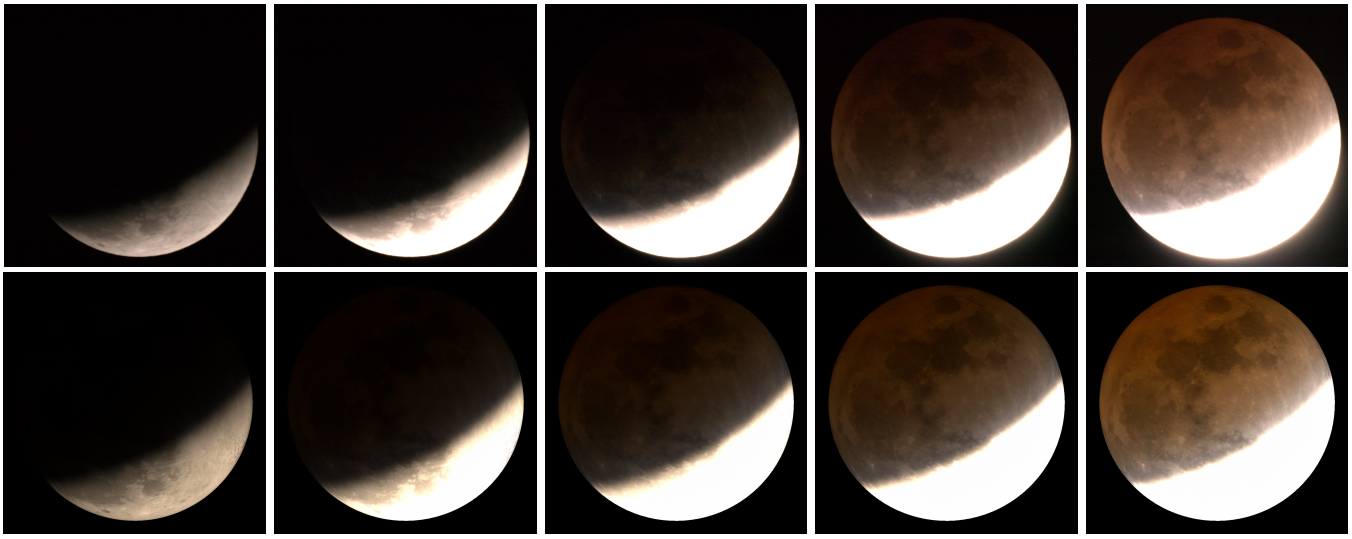

Figure 4: The top row shows a selection of photographs of the February 21st, 2008 eclipse at approximately 04:12:44 UTC; the bottom row shows our corresponding renderings. At this time the moon is in partial eclipse. The exposure times in seconds for these photographs and simulations are: 0.008, 0.050, 0.166, 0.500, and 1.509.

renderings of the eclipse from vantage points elsewhere in space would benefit from a bump-mapped approach, however.

The appearance of the moon for an earthly observer is also influenced by Rayleigh scattering on the path from the Moon back to Earth. The optical length of this path is a strong function of the angular position of the Moon in the sky; the path length at the horizon is about $40\times$ that at the zenith. This difference in path length causes two effects. First, the color of the Moon will be more red the closer it is to the horizon; this effect can be observed any time the Moon nears the horizon, not only during an eclipse. Additionally, due to refraction, the disk of the moon appears vertically flattened or "squished" near the horizon, similar to the appearance of sunsets, which have previously been modeled [35, 25]. We choose to model the color effects exclusively, since the distortion effects are apparent only very near the horizon. We calculate the optical depth (i.e. Rayleigh scattering coefficients at all the sampled wavelengths) for a column of air at the zenith by numerical integration of (7). Then we compute the relative optical air mass, $M(z_t)$, along a path as a function of true angle from the zenith, z_t [41]:

$$M(z_t) \approx \frac{1.002432\cos^2 z_t + 0.148386\cos z_t + 0.0096467}{\cos^3 z_t + 0.149864\cos^2 z_t + 0.01012963\cos z_t + 0.000303978}. \quad (14)$$

We multiply the relative optical air mass by the optical depth at the zenith to obtain an approximate optical depth at each wavelength. The resulting spectrum is used to filter the light reaching the Earth from the Moon. We note that although our curved ray tracer could be used to accurately model both the color and geometrical effects of the Moon-Earth light path, our chosen method is significantly faster and produces accurate renderings for all eclipses not very near the horizon.

The final element that must be simulated to accurately match eclipse appearance is the effect of atmospheric ozone (O_3). Ozone preferentially absorbs orange wavelengths in the so-called Chappuis band [26, 16]. Although many models of atmospheric ozone distributions have been proposed, we have found that a simple model works well in practice. We model these effects using a single spectral filter which accounts for the total mass of ozone in the atmosphere.

4 Results

4.1 Performance Details

To render the high-quality images shown in this paper, we traced 10^7 photons from the Sun, then replicated each one 100 times using symmetry. Computation of the photons took approximately 80 minutes on a 2.4Ghz Athlon 64 processor, using only a single core. The photon tracing algorithm is embarrassingly parallel, however, and times were reduced to just over 20 minutes on a quad-core machine. Shorter renderings were also tried, with 10^6 photons completing in around 8 minutes, and producing usable, if sometimes subtly banded or splotchy, illumination. For online visualization, these renderings are sufficient. Only one set of photons need be generated to render all views of a particular eclipse.

Calculation of the illumination map, including Monte Carlo estimation of the direct illumination component, takes about 20s per image on the same (single-core) processor. Once the pre-lit texture map has been generated, it can be viewed in real time.

4.2 Lunar Eclipse Photographic Comparison

For validation of our model, we compare the results to a series of digital photographs taken by the authors during the total lunar eclipse of February 21, 2008. We used predicted eclipse timings to set the date and time of deepest totality for photon generation. To model particular images, the date and time of our model were set according to the EXIF timestamp of the actual photographs. The photographs presented in the paper were captured in Clifton Park, New York and thus we used the same latitude and longitude to prepare the corresponding simulations.

We used a 127mm Maksutov-Cassegrain telescope of 1540mm focal length coupled to a Canon digital SLR camera to capture images at 3072×2048 resolution. The camera sensitivity was set to ISO-800, and an equatorial tracking mount allowed for sharp photographs of between $1/125$s and 8s duration. Photographs were taken in RAW mode, storing 12-bit samples at each Bayer site with no color conversion applied. To compare the digital photographs to the rendered images, we decoded the images into sRGB color space with a D65 white point using the open-source `dcraw` [6] program.

Shown in Figure 4 are a set of photographs with different exposure lengths taken at approximately the same time during the eclipse. Also shown are renderings produced by our model for

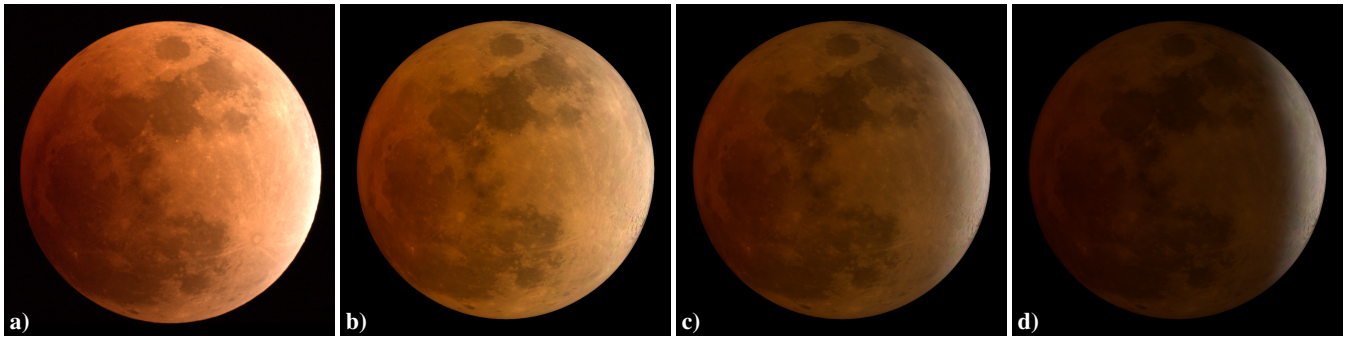

Figure 5: a) A photograph at 3:08:26 UTC of the 2008 eclipse in totality. Equivalent renderings with b) No dust ($\alpha = 0$) to mimic a Danjon L4 eclipse, c) light aerosol attenuation $\alpha = 4.7 \times 10^{-6}$ to mimic an L2 eclipse, and d) a heavy dust particulate ($\alpha = 1.0 \times 10^{-5}$) to mimic an L1 eclipse. The exposure for all images is 4.0s.

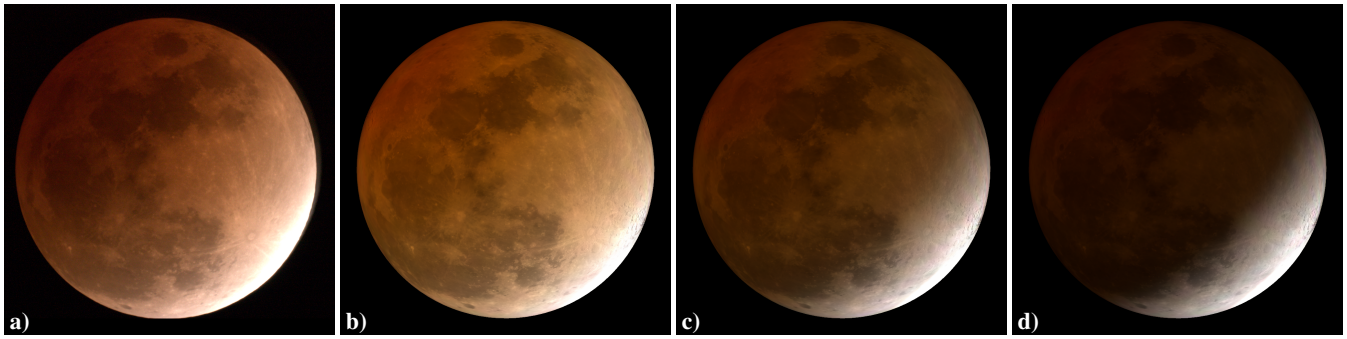

Figure 6: a) A photograph at 3:50:42 UTC of the 2008 eclipse near totality. Equivalent renderings with b) No dust ($\alpha = 0$) to mimic a Danjon L4 eclipse, c) light aerosol attenuation $\alpha = 4.7 \times 10^{-6}$ to mimic an L2 eclipse, and d) a heavy dust particulate ($\alpha = 1.0 \times 10^{-5}$) to mimic an L1 eclipse. The exposure for all images is 3.0s.

equivalent synthetic time and exposure settings, and using the default parameter for the stratospheric attenuation, α. As shown, the rendered images capture the qualitative look of the lunar eclipse well, including matching intensity ratios and approximate color. Subtle color differences between the images are noticeable, most likely because we did not model the exact state of the atmosphere at the time of the eclipse. Given the great variability in eclipse appearance represented on the Danjon scale (Section 1.1), however, these differences are plausibly within natural ranges.

Figures 5 and 6 show example renderings produced by varying the parameters of our model. We can obtain images roughly corresponding to descriptions for several levels on the Danjon scale. Although a great range of eclipse appearances can be rendered with our model, more experiments are required to determine if the entire range of observable eclipses can be obtained.

Finally, in Figure 7, we present predicted renderings of the December 2010 lunar eclipse from the same geographic location, assuming no significant atmospheric dust. An important aspect of lunar eclipse shadow measurements is the so-called "umbral enlargement", an observed phenomenon in which the exact timings of shadows crossing known crater features on the moon seem to indicate that the Earth's shadow is approximately 2% larger than predicted by geometry [11, 7]. Competing theories for this phenomenon include light lost due to refraction in the environment, or simple optical illusion [27]. The presented simulation and rendering method may prove useful to this ongoing investigation.

5 Conclusion and Future Work

We have presented a simple and efficient model and implementation for the color and intensity variations that are observed during partial and total lunar eclipses. This physically-based model takes into account atmospheric refraction, scattering, and attenuation using physical measured data and models when available. Our results are compared to photographs of the recent 2008 total lunar eclipse.

A wealth of images of eclipses dating back at least 100 years taken by amateur and professional astro-photographers can be found online. Careful color normalization of these images to allow validation of our model is an interesting and significant challenge for future investigation. Although records of weather and atmospheric aerosol conditions at the time of each eclipse are incomplete, it may be possible to deduce these conditions through simulation and comparison with the photographs.

Acknowledgements

The authors would like to thank the committee and anonymous reviewers for their helpful comments and suggestions during the submission process. The authors were supported by Rensselaer Polytechnic Institute for this research.

References

[1] *IEC/4WD 61966-2-1: Colour Measurement and Management in Multimedia Systems and Equipment - Part 2-1: Default RGB Colour Space - sRGB*. International Electrotechnical Commission, 1998.

[2] American Society for Testing and Materials. Standard ASTM E490-2000, Standard for Solar Constant and Air Mass Zero Solar Spectral Irradiance Tables, 2000.

[3] M. Berger, T. Trout, and N. Levit. Ray tracing mirages. *IEEE Comput. Graph. Appl.*, 10(3):36–41, 1990.

[4] A. Bucholtz. Rayleigh-scattering calculations for the terrestrial atmosphere. *Appl. Opt.*, 34(15):2765–2773, 1995.

[5] CIE. *Commission Internationale de l'Eclairage Proceedings, 1931*. Cambridge University Press, Cambridge, 1932.

[6] D. Coffin. dcraw: Decoding raw digital photos in Linux, 2008. `http://www.cybercom.net/~dcoffin/dcraw/`.

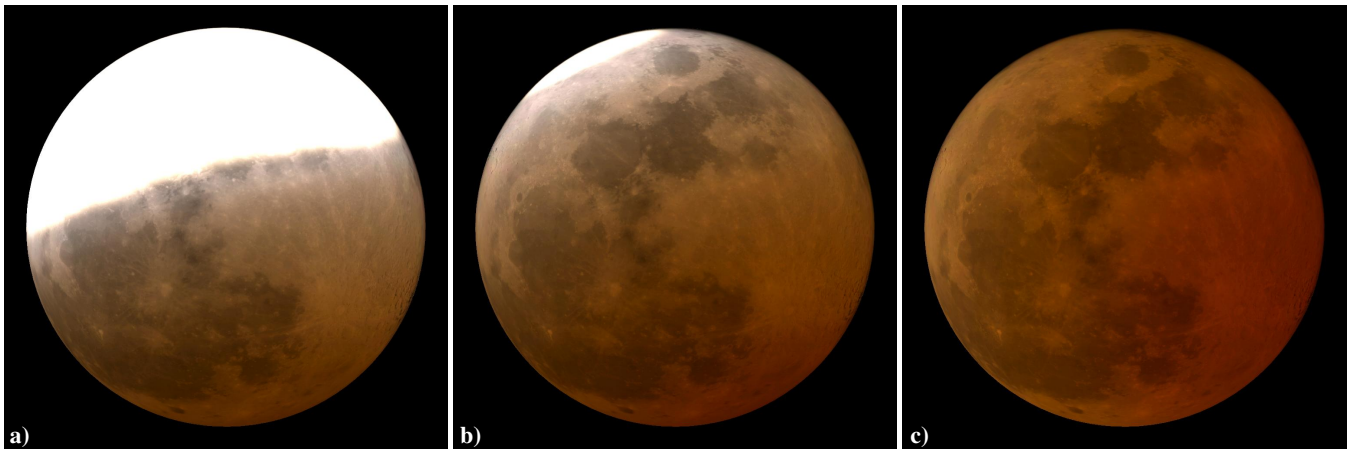

Figure 7: Using the simulation and rendering method presented in this paper, we predict imagery of the December 21, 2010 lunar eclipse viewed from upstate New York a) at 7:22:17 UTC in partial eclipse, b) at 7:40:21 UTC near totality, and c) at 8:16:56 UTC in deepest totality. These predictions assume a no dust atmosphere resulting in a Danjon L4 eclipse. The exposure for the images are 0.8, 1.0, and 1.5 seconds respectively.

[7] T. P. Cooper and M. Geyser. Size and shape of the umbra during a lunar eclipse. *Monthly Notes of the Astronomical Society of Southern Africa*, 63:12.

[8] T. P. Cooper and M. Geyser. Size and shape of the umbra during a lunar eclipse. *Monthly Notes of the Astron. Soc. Southern Africa*, 63:12–19, 2004.

[9] *Handbook of Chemistry and Physics*. CRC Press, Cleveland, Ohio, 1984.

[10] A. Danjon. *Comptes Rendues*, 171:1127–1207, 1920.

[11] F. Espenak and J. Meeus. Five millennium catalog of lunar eclipses: -1999 to +3000. Technical Report TP-2009-214173, NASA.

[12] A. Glassner. *Principles of Digital Image Synthesis*, volume 1 and 2. Morgan-Kaufmann, 1995.

[13] D. Gutierrez, A. Muñoz, O. Anson, and F. J. Serón. Non-linear volume photon mapping. In *Rendering Techniques*, pages 291–300, 2005.

[14] D. Gutierrez, F. Seron, O. Anson, and A. Munoz. Chasing the green flash: a global illumination solution for inhomogeneous media. *Proceedings of the 20th spring conference on Computer graphics*, April 22-24 2004.

[15] D. Gutierrez, F. J. Seron, A. Munoz, and O. Anson. Simulation of atmospheric phenomena. *Computers & Graphics*, 30(6):994–1010, Dec. 2006.

[16] J. Haber, M. Magnor, and H.-P. Seidel. Physically-based simulation of twilight phenomena. *ACM Trans. Graph.*, 24(4):1353–1373, 2005.

[17] J. Hansen and S. Matsushima. Light illuminance and color in the earth's shadow. *J. Geophys. Rev.*, 71:1073–1081, 1966.

[18] N. Hernitschek, E. Schmidt, and M. Vollmer. Lunar eclipse photometry: absolute luminance measurements and modeling. *Appl. Opt.*, 47(34):H62–H71, 2008.

[19] D. Hoffman, J. Barnes, E. Dutton, T. Deshler, H. Jäger, R. Keen, and M. Osborn. Surface-based observations of volcanic emissions to the stratosphere. *Geophysical monograph*, pages 57–73, 2003.

[20] H. Jensen, D. F., M. Stark, S. Premoze, J. Dorsey, and P. Shirley. A physically-based night sky model. In E. Fiume, editor, *SIGGRAPH 2001, Computer Graphics Proceedings*, pages 399–408. ACM Press / ACM SIGGRAPH, 2001.

[21] H. Jensen, S. Premoze, P. Shirley, W. Thompson, J. Ferwerda, and M. Stark. Night rendering. Technical Report UUCS-00-016, University of Utah, Computer Science Department, August 2000.

[22] R. A. Keen. Volcanic aerosols and lunar eclipses. *Science*, 222(4627):1011–1013, 1983.

[23] J. Kepler. *Astronomiae Pars Optica*. 1604.

[24] R. V. Klassen. Modeling the effect of the atmosphere on light. *ACM Trans. Graph.*, 6(3):215–237, 1987.

[25] A. Linţu, J. Haber, and M. Magnor. Realistic Solar Disc Rendering. In *WSCG'2005 Full Papers Conference Proceedings*, pages 79–86, Feb. 2005.

[26] F. Link. *Eclipse Phenomena in Astronomy*. Springer-Verlag, 1969.

[27] P. Marmet and C. Couture. Enlargement of the earth's shadow on the moon: An optical illusion, Last accessed: March 2009. `http://www.newtonphysics.on.ca/Astronomy/Astronomy.htm`.

[28] S. Matsushima, J. R. Zink, and J. E. Hansen. Atmospheric extinction by dust particles as determined from three-color photometry of the lunar eclipse of 19 December 1964. *Astronomical Journal*, 71:103–110, Mar. 1966.

[29] J. Meeus. *Astronomical Formulae for Calculators*. Willman-Bell, Inc., fourth edition, 1988.

[30] J. Meeus. *Astronomical Algorithms*. Willman-Bell, Inc., second edition, 1998.

[31] M. Minnaert. *The Nature of Light and Colour in the Open Air*. Dover, 1954.

[32] T. Nishita, T. Sirai, K. Tadamura, and E. Nakamae. Display of the earth taking into account atmospheric scattering. *Proceedings of the 20th annual conference on Computer graphics and interactive techniques*, pages 175–182, 1993.

[33] C. M. Pieters. The moon as spectral calibration standard enabled by lunar samples: The clementine example. In *Workshop on New Views of the Moon II: Understanding the Moon through the Integration of Diverse Datasets*, pages 47–49, 1999.

[34] A. Preetham, P. Shirley, and B. Smits. A practical analytic model for daylight. In A. Rockwood, editor, *Siggraph 1999, Computer Grahics Procedings*, pages 91–100, Los Angeles, 1999. Addison Wesley Longman.

[35] F. Seron, D. Gutierrez, G. Gutierrez, and E. Cerezo. Visualizing sunsets through inhomogeneous atmospheres. In *Computer Graphics International 2004*, pages 349–356, June 2004.

[36] J. Stam and E. Languenou. Ray tracing in non-constant media. In X. Pueyo and P. Schroeder, editors, *RenderingTechniques '96, Proceedings of the 7th Eurographics Workshop on Rendering*, pages 225–234. Springer-Verlag, 1996.

[37] R. B. Stothers. Stratospheric Transparency Derived from Total Lunar Eclipse Colors, 1801-1881. *The Publications of the Astronomical Society of the Pacific*, 117:1445–1450, Dec. 2005.

[38] *U.S. Standard Atmosphere*. U.S. Government Printing Office, 1976.

[39] S. Y. van der Werf. Ray tracing and refraction in the modified us1976 atmosphere. *Appl. Opt.*, 42(3):354–366, 2003.

[40] M. Vollmer and S. D. Gedzelman. Simulating irradiance during lunar eclipses: the spherically symmetric case. *Appl. Opt.*, 47(34):H52–H61, 2008.

[41] A. T. Young. Air mass and refraction. *Appl. Opt.*, 33(6):1108–1110, 1994.